ELSEVIER

Journal of Hazardous Materials B134 (2006) 94–103

Journal of Hazardous Materials

www.elsevier.com/locate/jhazmat

Aqueous Cr(VI) photo-reduction catalyzed by TiO_2 and sulfated TiO_2

Fang Jiang, Zheng Zheng, Zhaoyi Xu, Shourong Zheng *, Zhaobing Guo, Liqiang Chen

State Key Laboratory of Pollution Control and Resource Reuse, School of the Environment, Nanjing University, Nanjing 210093, PR China

Received 23 September 2005; received in revised form 16 October 2005; accepted 18 October 2005
Available online 28 November 2005

Abstract

TiO_2 and sulfated TiO_2 (SO_4^{2-}/TiO_2) catalysts with different textural properties were prepared under different calcination temperatures and the photo-reduction of Cr(VI) to Cr(III) catalyzed by these catalysts was investigated. For the photocatalytic reduction of Cr(VI), the photocatalytic activities of the TiO_2 samples were found to be strongly dependent of the calcination temperature and TiO_2 calcined at 400 °C showed a higher catalytic activity compared to other TiO_2 catalysts. In contrast, sulfation of TiO_2 stabilized the catalytic activities of SO_4^{2-}/TiO_2 catalysts. At low calcination temperature, SO_4^{2-}/TiO_2 catalysts exhibited catalytic activities almost comparable with that of TiO_2 and the catalytic activities of SO_4^{2-}/TiO_2 catalysts were markedly higher than TiO_2 under high calcination temperature. In addition, the removal of surface SO_4^{2-} of SO_4^{2-}/TiO_2 catalyst led to a marked decrease of the catalytic activity for Cr(VI) photo-reduction, suggesting that the presence of surface SO_4^{2-} provided an acid environment over the catalyst surface and favored the photo-reduction of Cr(VI).

Keywords: TiO_2; Sulfated TiO_2; Surface acidity; Cr(VI) photo-reduction; Photocatalysis

1. Introduction

As one of the advanced oxidation processes (AOPs), photocatalytic abatement of pollutants has attracted considerable interest from both academic and industrial societies [1–3]. TiO_2 photocatalyst was considered as one of the most practical candidates due to its high stability and photocatalytic efficiency [4–6]. Recently, much attention has been paid to modifying TiO_2 to enhance its catalytic efficiency or expand its applicability under solar irradiation [7–9].

Modification of TiO_2 via sulfation has been proved to be an effective approach to enhance its catalytic efficiency. Gómez et al. [10] studied the photocatalytic degradation of 2,4-dinitroaniline and observed that SO_4^{2-}/TiO_2 showed a higher catalytic activity compared to TiO_2. Samantaray et al. [11] also found that 4-nitrophenol could be effectively decomposed in the presence of SO_4^{2-}/TiO_2. In general, sulfation of TiO_2 can cause marked changes in the specific surface area, crystallinity, crystalline transformation and surface acidity of TiO_2, which may control its catalytic activity. However, the influence of surface SO_4^{2-} on the photocatalytic performance of sulfated TiO_2 is still in controversy. Colón et al. [12] studied the degradation of phenol and concluded that the enhanced catalytic activity was not relative to the increased surface acidity of sulfated TiO_2.

The photocatalytic removal of pollutants is based on the excitation of electrons from the valence band to the conduction band of the semiconductor initiated by the light absorption [1,2,13]. In principle, the excited electrons or holes can be utilized to reduce or oxidize pollutants, respectively. For SO_4^{2-}/TiO_2 catalyst, most studies focused on the oxidation of pollutants using the excited holes [10–12,14–16]. However, the catalytic behavior of SO_4^{2-}/TiO_2 in the photo-reduction reactions, which is based on the utilization of the excited electrons, was seldom addressed [7] and the influence of its structural properties on the efficiency of photocatalytic reduction is still unclear.

Cr(VI) pollution has been found in the wastewater from industrial processes, such as mining, leather tanning, metal electroplating, paint making, etc. [17]. In a typical treatment process, Cr(VI) can be reduced to less toxic Cr(III) by reducing agents, such as ferrous sulfate and sodium bisulfite. The resulting Cr(III) in the wastewater can be removed subsequently by precipitation at neutral or alkaline pH. However, a larger dosage of the reducing agent than the stoichiometric amount has to be used in order to completely reduce Cr(VI) to Cr(III). As an environment-friendly treatment process, photocatalytic reduction has been

* Corresponding author. Tel.: +86 25 83595831; fax: +86 25 83707304.
E-mail address: srzheng@nju.edu.cn (S. Zheng).

0304-3894/$ – see front matter © 2005 Elsevier B.V. All rights reserved.
doi:10.1016/j.jhazmat.2005.10.041

explored and proved to be effective in the reduction of Cr(VI) to Cr(III) [1,18–22].

In this contribution, TiO_2 and SO_4^{2-}/TiO_2 catalysts with different properties were synthesized and the photo-reduction of Cr(VI) catalyzed by these catalysts was evaluated. The objective of this study is to investigate the dependence of the photocatalytic performance on their textural properties and the role of surface SO_4^{2-} in SO_4^{2-}/TiO_2 catalysts.

2. Experimental

2.1. Preparation of catalysts

TiO_2 precursor was prepared using the sol–gel method. In a typical synthesis, a mixture of 20 ml distilled water and 20 ml isopropanol was introduced into a mixture of 40 ml titanium tetraisobutyloxide and 200 ml isopropanol at room temperature with strong stirring. The resulting gel was then recovered by centrifugation followed by a distilled water rinse. Subsequently, TiO_2 precursor was obtained by drying at 80 °C for 12 h. TiO_2 samples with different properties were prepared by calcining the TiO_2 precursor at corresponding temperatures for 4 h.

SO_4^{2-}/TiO_2 was prepared by impregnating 1.0 g of TiO_2 precursor with 5 ml of 0.2 M H_2SO_4 for 24 h followed by drying at 80 °C. Different SO_4^{2-}/TiO_2 samples were obtained by calcining H_2SO_4 impregnated TiO_2 at different temperatures for 4 h. The resulting catalysts are labeled as TiO_2-*x* or SO_4^{2-}/TiO_2-*x*, where *x* denotes the calcination temperature (°C).

2.2. Surface treatment of sulfated TiO_2 with Na_2CO_3 solution

For the surface treatment of SO_4^{2-}/TiO_2-500, 1 g of SO_4^{2-}/TiO_2-500 was suspended in 100 ml of 0.5 M Na_2CO_3 solution at room temperature for 24 h in order to remove the surface SO_4^{2-}. The solid particles were then filtrated and rinsed repeatedly with distilled water till the eluent was neutral. The sample was subsequently dried at 80 °C for 12 h and the resulting sample is denoted as SO_4^{2-}/TiO_2-500-W.

2.3. Characterization

XRD patterns of the TiO_2 and SO_4^{2-}/TiO_2 samples were collected in a Rigaku D/max-RA powder diffraction-meter using Cu Kα radiation. To determine the content of anatase and rutile in the samples, quantitative XRD measurements were carried out using the inter-standard method [23]. As the standard TiO_2 sample with known crystallinity degree is unavailable, TiO_2 calcined at 950 °C for 4 h contained pure rutile phase and was considered as the reference sample with approximately 100% crystallinity degree. For the sample containing only anatase phase, the catalyst sample was physically mixed with the reference TiO_2 sample (50 wt.%/50 wt.%) by repeated grinding and the mixture was then charged for XRD analysis. Considering that the intensity of XRD diffraction peak is proportional to the mass fraction of the related crystalline phase, the ratio of anatase mass fraction to rutile mass fraction in the mixture was calculated as follows [24]:

$$W_A/W_R = 0.886A_A/A_R \quad (1)$$

where W_A and W_R represent the weight fractions of anatase and rutile, A_A and A_R are the integrated intensities of the anatase(1 0 1) peak and rutile(1 1 0) peak, respectively.

As the content of rutile in TiO_2-950 was considered as 100% and the ratio of sample mass to TiO_2-950 mass was 1:1 in this mixture, the content of anatase in the sample can be thus obtained:

$$\text{anatase}\,(\%) = (0.886A_A/A_R) \times 100 \quad (2)$$

For the sample containing rutile phase or mixed anatase and rutile phases, CuO was used as the internal standard. Typically, the sample or the reference TiO_2-950 was physically mixed with CuO internal standard (50 wt.%/50 wt.%) and the mixture was then charged for XRD analysis. The resulting XRD spectra were normalized based on the strongest peak of CuO. The crystalline contents of rutile and anatase phases in the samples were obtained by comparing their normalized XRD spectra with the normalized spectra of TiO_2-950.

The thermogravimetric (TG) analysis of the samples was conducted on a NETZSCH STA 449C instrument from 20 to 800 °C with an increment of 10 °C/min. The BET surface area was determined by N_2 adsorption on a Micrometrics ASAP 2020 apparatus at −196 °C (77 K).

The acidic properties of the catalysts were characterized using NH_3 temperature programmed desorption (NH_3-TPD) and IR spectroscopy of pyridine adsorption. For NH_3-TPD, 100 mg of sample was pressed into wafers, broken into small pellets and charged into a quartz reaction tube. The sample was then activated under N_2 flow by heating at 450 °C for 1 h. After cooling the sample to 100 °C, NH_3 adsorption was carried out. Physically adsorbed NH_3 was removed by N_2 purging at 150 °C for 1 h. NH_3-TPD of the sample was carried out by heating the sample from 150 to 450 °C at a rate of 10 °C/min. The amount of NH_3 desorbed was quantitatively monitored with a TC detector.

For pyridine adsorption, a self-supporting wafer of the sample was placed in a sample holder in the center of a furnace, which was connected to a vacuum system. During activation the sample was heated in vacuo (<10^{-5} mbar) to 400 °C with a rate of 10 °C/min and kept at this temperature for 2 h. The adsorption of pyridine was carried out at a partial pressure of 2×10^{-2} mbar using an equilibration time of 15 min. After removing physically adsorbed molecules by degassing at 150 °C for 1 h, IR spectra were collected at room temperature with 4 cm^{-1} resolution using a Vector 22 FT-IR spectrometer. In order to allow quantitative comparisons of the band intensities, the used sample wafers were weighted and the spectra were normalized based on the mass of the wafer.

2.4. Cr(VI) adsorption isotherms

Cr(VI) adsorption isotherms over the catalysts were obtained using the static adsorption method. Typically, pH value of Cr(VI)

solution was adjusted to 2.5 with sulfuric acid prior to the adsorption experiments. 0.05 g of catalyst was suspended in 50 ml Cr(VI) solution in 100 ml conical flasks with initial concentrations ranging from 1 to 60 mg/l. The conical flasks were shaken in the dark at 20 °C for 12 h. The catalyst powders were removed by filtration and the residual concentration of Cr(VI) in the solution was determined spectraphotometrically using diphenylcarbazide as the color agent. Under our experimental conditions, the difference of Cr(VI) concentration before and after adsorption on TiO_2-600 and TiO_2-700 was almost undetectable due to their especially small adsorption capacities. Therefore, only the isotherms of Cr(VI) adsorption on TiO_2-300, TiO_2-400 and TiO_2-500 were measured in this study.

2.5. Photocatalytic activity

The catalytic activities of the catalysts for Cr(VI) photo-reduction were investigated. Cr(VI) photo-reduction was carried out in a NDC photo-reactor equipped with a 500 ml thermostatted cylindrical Pyrex vessel irradiated directly by a high pressure mercury lamp (500 W), which is shown in Fig. 1. In a typical run, 0.5 g of the catalyst was suspended in 500 ml of 40 mg/l Cr(VI) solution with pH 2.5 in the dark for 100 min to reach the adsorption equilibrium prior to the photo-reduction experiment. During the photo-reaction, samples were collected at selected time intervals. The catalyst powders were removed by filtration and the residual concentration of Cr(VI) was determined spectra-photo-metrically.

3. Results and discussion

3.1. Catalyst characterization

The quantitative analysis of the crystalline phase content in the TiO_2 and sulfated TiO_2 samples was conducted and the results are summarized in Fig. 2. The crystalline phases of TiO_2-300 and TiO_2-400 were found to be pure anatase and the crystalline phases of TiO_2-500 were anatase and rutile. Increasing the calcination temperature from 300 to 400 °C led to the increase of the anatase content from 18% to 25%. As the calcination temperature increased from 500 to 700 °C, the content of rutile was significantly increased in the TiO_2 samples. In contrast, only anatase phase was detected in the SO_4^{2-}/TiO_2 samples prepared at the calcination temperature below 700 °C. In addition, the content of anatase in SO_4^{2-}/TiO_2-300 and SO_4^{2-}/TiO_2-400 was found to be approximately 8% and 11%, respectively, which indicates that the presence of SO_4^{2-} on the surface of TiO_2 retards the transformation of TiO_2 crystalline phases from amorphous to anatase and from anatase to rutile. The results are in good agreement with previous reports [11,12].

The average crystallite sizes of the TiO_2 and sulfated TiO_2 samples can be estimated based on XRD patterns using the Scherrer formula [25] and the results as well as BET surface areas are compared in Table 1. Under the same calcination temperature, the crystallite sizes of the TiO_2 samples were found to be larger than those of the SO_4^{2-}/TiO_2 samples, which suggests that the presence of SO_4^{2-} on the surface of TiO_2 also hinders the growth of TiO_2 crystallites. In parallel, increasing the calcination

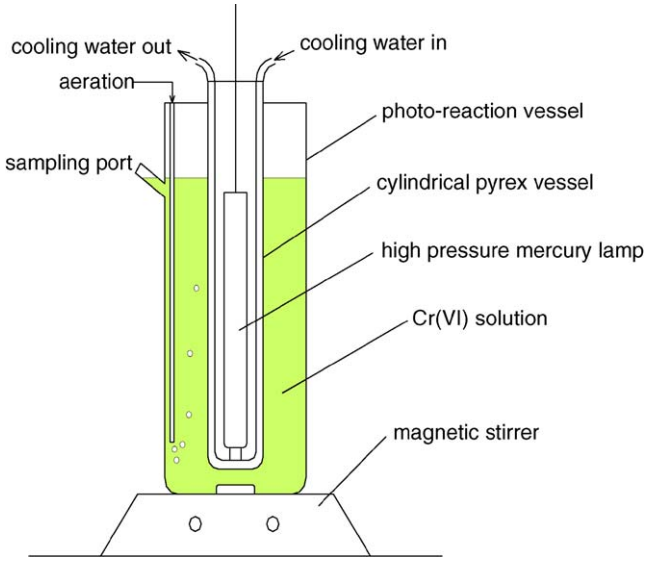

Fig. 1. Schematic diagram of photo-reactor.

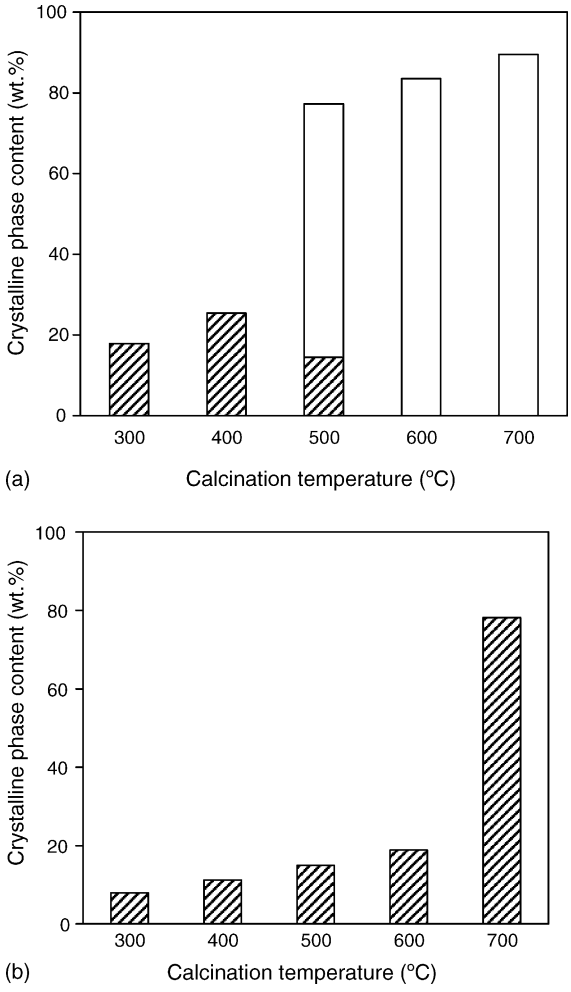

Fig. 2. Crystalline phase content of (a) TiO_2 and (b) sulfated TiO_2. Striped columns: anatase phase; white columns: rutile phase.

Table 1
Average crystallite sizes and BET specific surface areas of TiO_2 and sulfated TiO_2 samples

Sample	Crystallite size (nm)	BET surface area (m^2/g)
TiO_2-300	8.8	115.3
TiO_2-400	13.6	89.2
TiO_2-500	44.1	45.0
TiO_2-600	58.2	6.5
TiO_2-700	59.4	2.0
SO_4^{2-}/TiO_2-300	5.7	191.8
SO_4^{2-}/TiO_2-400	6.0	171.2
SO_4^{2-}/TiO_2-500	6.2	143.6
SO_4^{2-}/TiO_2-600	10.3	72.6
SO_4^{2-}/TiO_2-700	31.3	22.5

temperature from 300 to 700 °C also led to the decrease of the specific surface areas of TiO_2 samples from 115.3 to 2.0 m^2/g. Note that the specific surface area of the sulfated TiO_2 sample is larger compared to that of TiO_2 sample under similar calcination conditions, demonstrating that surface SO_4^{2-} suppresses the aggregation of TiO_2 particles during the calcination procedure.

TG curves of the TiO_2 precursor and TiO_2 precursor impregnated with SO_4^{2-} are presented in Fig. 3. The total weight losses of TiO_2 and sulfated TiO_2 in the temperature region between 50 and 350 °C were 11.2% and 11.4%, respectively, which is ascribed to water desorption from the samples. For TiO_2, no further weight loss was observed at temperature higher than 350 °C. In contrast, approximately 6.6% of total weight of the sulfated TiO_2 sample was further loosed from about 500 °C to 750 °C, which could be attributed to the decomposition/desorption of SO_4^{2-} species on the surface of TiO_2 at high calcination temperatures [26].

3.2. Cr(VI) adsorption isotherms

In a hetero-catalytic reaction system, the catalytic reaction basically occurs on the surface of the catalyst. At the same time, it was always observed that most of photocatalytic reactions followed Langmuir–Hinshelwood model [27–30], which also suggests that the adsorption of reactants onto the surface of the catalyst controls the photocatalytic efficiency. Therefore, information about the adsorption of reactants on the surface of the catalyst is very important for understanding the photocatalytic performance of the catalyst.

Cr(VI) adsorption isotherms on the TiO_2 and sulfated TiO_2 samples at pH 2.5 and 20 °C are presented in Fig. 4. The adsorption behaviors of Cr(VI) on the samples could be well described by the Langmuir adsorption model [31]:

$$Q_e = Q_0 b C_e/(1 + bC_e) \quad (3)$$

where Q_e is the equilibrium adsorption amount (mg/g), Q_0 the maximum adsorption amount (mg/g), b the adsorption constant (l/mg) and C_e the equilibrium concentration of Cr(VI) (mg/l), respectively.

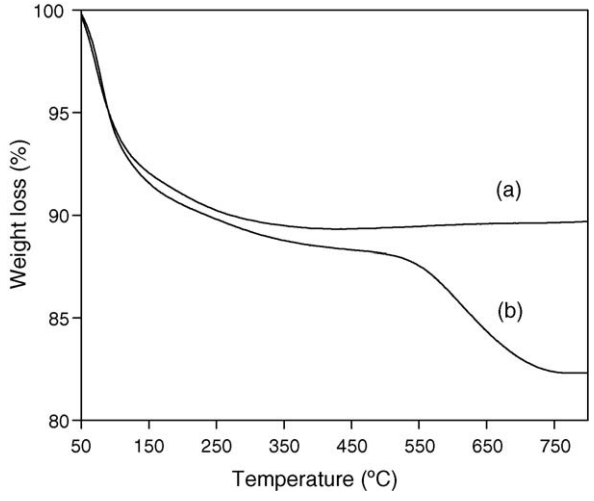

Fig. 3. Thermogravimetric (TG) curves of (a) TiO_2 and (b) sulfated TiO_2 precursors.

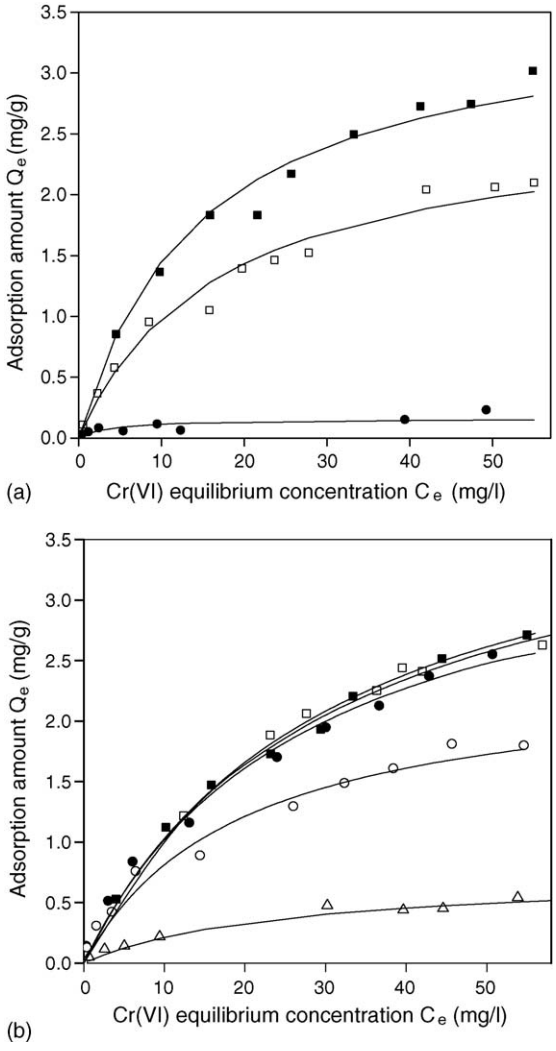

Fig. 4. Adsorption isotherms of Cr(VI) on (a) TiO_2 and (b) sulfated TiO_2 samples calcined at different temperatures: (■) 300 °C, (□) 400 °C, (●) 500 °C, (○) 600 °C, (△) 700 °C. Solid lines are theoretical fitting curves using Langmuir adsorption model.

Table 2
Parameters of Cr(VI) adsorption on TiO_2 and sulfated TiO_2 samples

Sample	Q_0 (mg/g)	b (l/mg)
TiO_2-300	3.55	0.07
TiO_2-400	2.25	0.10
TiO_2-500	0.16	0.25
SO_4^{2-}/TiO_2-300	4.25	0.03
SO_4^{2-}/TiO_2-400	4.15	0.03
SO_4^{2-}/TiO_2-500	3.93	0.04
SO_4^{2-}/TiO_2-600	2.40	0.05
SO_4^{2-}/TiO_2-700	0.77	0.05

Q_0: the maximum adsorption amount; b: the adsorption constant.

The parameters of Cr(VI) adsorption on the catalysts, obtained by fitting the experimental data using the Langmuir adsorption model, are listed in Table 2. For TiO_2 samples, increasing the calcination temperature from 300 to 500 °C led to a decrease of the maximum adsorption amount from 3.55 to 0.16 mg/g. In parallel, increasing the calcination temperature from 300 to 700 °C resulted in a decrease of the maximum adsorption amount of the SO_4^{2-}/TiO_2 samples from 4.25 to 0.77 mg/g. The lower adsorption amount of the sample calcined at higher temperature could be ascribed to the growth of the crystallites, decrease of the specific surface area and/or decrease of the density of the adsorption sites of the catalyst. This conclusion is in good agreement with XRD results. Note that the presence of surface SO_4^{2-} attenuates the dependence of the adsorption amounts of the SO_4^{2-}/TiO_2 samples on the calcination temperatures compared with that of the TiO_2 samples.

In principle, the adsorption amount of Cr(VI) on TiO_2 or sulfated TiO_2 catalyst is relative to its specific surface area and density of the surface adsorption sites. The ratio of Cr(VI) maximum adsorption amount to the specific surface area, defined as D (mg/m^2), reflects the density of the surface adsorption sites of the catalyst. The dependence of D values on the calcination temperature is described in Fig. 5. For TiO_2, a marked decrease of the ratio was observed with the increase of the calcination temperature, which suggests that increasing the calcination temperature leads to the decrease in the density of the adsorption sites on the surface of TiO_2. In contrast, a slight increase of the ratio for the SO_4^{2-}/TiO_2 samples was observed with the increase of the calcination temperature.

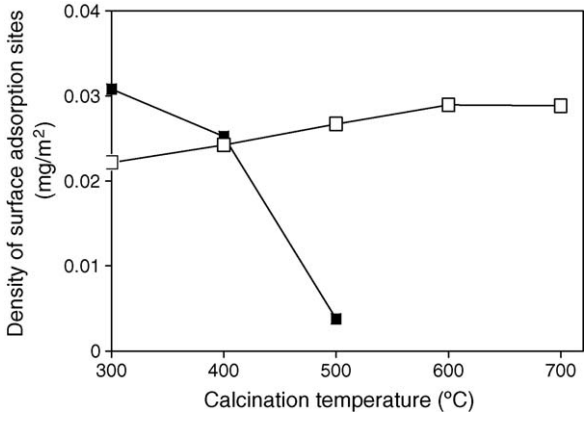

Fig. 5. The dependence of density of adsorption sites on the calcination temperature: (■) TiO_2 and (□) sulfated TiO_2.

Generally, the hydroxyl groups on the surface of TiO_2 and sulfated TiO_2 are considered as the Cr(VI) adsorption sites [32]. At pH 2.5, Cr(VI) exits in the solution as $HCrO_4^-$, CrO_4^{2-} or $Cr_2O_7^{2-}$ [33]. Furthermore, the surface of catalyst is positively charged at pH 2.5 as pH_{zpc} of TiO_2 was reported to be 6.15 [34], which suggests that Cr(VI) species are adsorbed on the surface of the catalysts via a electrostatic interaction. Boehm and Herrmann [35] observed that the density of the hydroxyl groups of TiO_2 depended on the calcination temperature. López et al. [36] used IR spectroscopy to characterize the influence of the calcination on the hydroxyl groups of TiO_2 and also found that increasing the calcination temperature led to the dehydroxylation of TiO_2 surface. Therefore, the continuous decrease of the density of the adsorption sites on the surface of TiO_2 is essentially related to the increase of the calcination temperature. For the SO_4^{2-}/TiO_2 samples, increasing the calcination temperature led to a slight increase of the density of the adsorption sites, indicating that the presence of SO_4^{2-} preserves the surface hydroxyl groups of the sulfated TiO_2 samples. This clearly indicated that the decrease of Cr(VI) maximum adsorption capacities of the TiO_2 samples were resulted from both their increased crystallite sizes and the decreased densities of the surface adsorption sites. However, the decreased maximum adsorption amounts of the SO_4^{2-}/TiO_2 samples are mainly due to their decreased specific surface areas.

3.3. Photocatalytic activity

In the presence of photocatalyst, Cr(VI) can be reduced to Cr(III) by the excited electrons initiated by UV irradiation. The overall reaction of Cr(VI) photo-reduction could be described as follows [37,38]:

$$Cr_2O_7^{2-} + 14H^+ + 6e^- \rightarrow 2Cr^{3+} + 7H_2O \quad (4)$$

$$2H_2O + 4h^+ \rightarrow O_2 + 4H^+ \quad (5)$$

The time profiles of Cr(VI) photo-removal catalyzed by the TiO_2 and SO_4^{2-}/TiO_2 samples are compared in Fig. 6. The results indicated that TiO_2-400 had a slightly higher catalytic activity compared to TiO_2-300. At the calcination temperature higher than 400 °C, the catalytic efficiency of TiO_2 markedly diminished with the increase of the calcination temperature. In contrast, no marked difference in the catalytic efficiencies was observed for the SO_4^{2-}/TiO_2 samples prepared at the calcination temperature lower than 600 °C. Calcination of SO_4^{2-}/TiO_2 at 700 °C led to a marked decrease of the catalytic activity.

Typically, the photocatalytic removal of inorganic and organic pollutants follows Langmuir–Hinshelwood model [27–30]. For Cr(VI) photo-reduction, Ku and Jung [33] observed that Cr(VI) photo-reduction fitted first-order reaction kinetics. Our fitting results also showed that the kinetics of Cr(VI) photo-reduction catalyzed by different catalysts could be well described as pseudo-first-order kinetics:

$$r = -dC_t/dt = K_{app}C_t \quad (6)$$

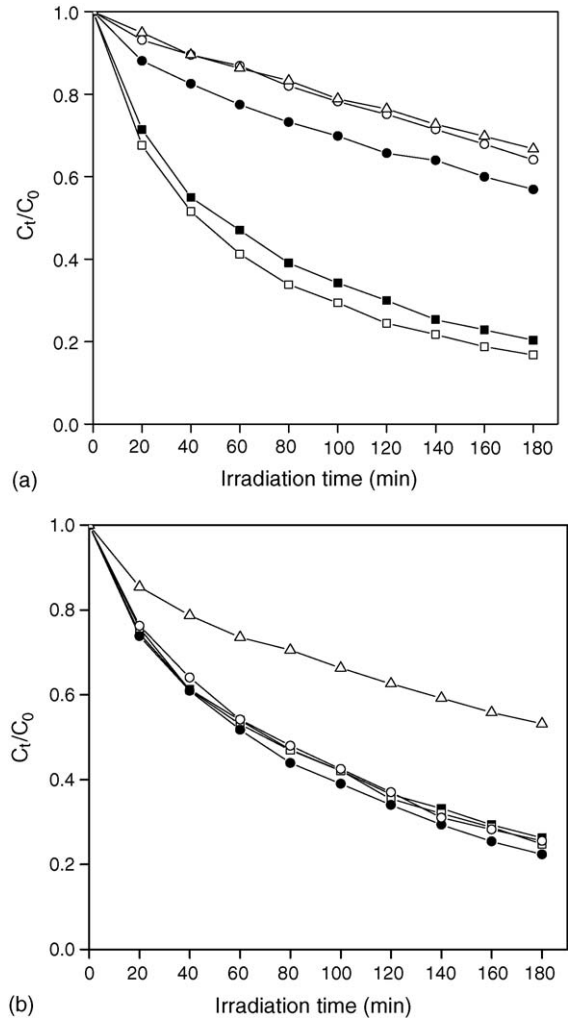

Fig. 6. Photo-reduction of Cr(VI) catalyzed by (a) TiO_2 and (b) sulfated TiO_2 samples calcined at different temperatures: (■) 300 °C, (□) 400 °C, (●) 500 °C, (○) 600 °C, (△) 700 °C. The pH value of solution was 2.5, initial concentration of Cr(VI) ion was 40 mg/l, dosage of catalyst was 1 g/l.

$$\ln(C_0/C_t) = K_{app}t \quad (7)$$

where C_o denotes the initial concentration of Cr(VI) (mg/l), C_t the concentration of Cr(VI) at reaction time t and K_{app} is the apparent rate constant (min^{-1}), respectively.

The apparent rate constants of the catalysts for Cr(VI) photo-reduction, obtained by fitting the experimental data, are compared in Fig. 7. In general, the specific surface area, the crystalline phases and the crystallinity degree of the photocatalyst were believed to be the most important factors controlling its photocatalytic activity [39]. In principle, the large specific surface area of the catalyst implies high adsorption capacity. Ohtani et al. [40] observed that the photocatalytic activity was proportional to the reactant concentration on the catalyst surface. Furthermore, a large amount research results proved that Langmuir–Hinshelwood model were applicable to explain the kinetics of aqueous pollutant photo-degradation catalyzed by TiO_2 catalyst, demonstrating the dependence of the photocatalytic activity on the surface adsorption. For the influence of TiO_2 catalyst crystallinity, Sreethawong et al. [41] concluded

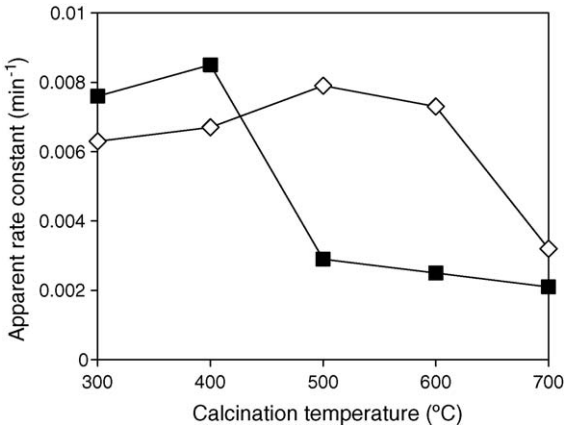

Fig. 7. The dependence of apparent rate constants of the catalysts on the calcination temperature: (■) TiO_2 and (□) sulfated TiO_2.

that high crystallinity of TiO_2 catalyst led to a low surface defects and effectively inhibited the recombination of electron–hole, which led to a higher catalytic activity. In addition, the photocatalytic activities also varied with different crystalline phases of TiO_2. Typically, anatase TiO_2 exhibited markedly higher catalytic activity compared to amorphous or rutile TiO_2 [23]. Recently, enhanced photocatalytic activity TiO_2 with mixed anatase and rutile phases were reported, which was attributed to the synergistic effect between anatase and rutile [42–44].

For Cr(VI) photo-reduction by TiO_2 catalysts, TiO_2-400 showed higher crystallinity and lower adsorption capacity compared to TiO_2-300. Therefore, the enhanced photocatalytic activity of TiO_2-400 is ascribed to the increased content of anatase compared with that of TiO_2-300. Although calcination of TiO_2 at 500 °C led to an increased content of crystalline phases and the presence of the mixed anatase and rutile phases, the marked decrease of the adsorption capacity of TiO_2-500 for Cr(VI) resulted in the decrease of the photocatalytic activity. Further increasing the calcination temperature led to the continuous decrease of Cr(VI) adsorption capacity and the phase transformation from anatase to rutile, which accounted for the continuously decreased catalytic activities of these TiO_2 catalysts.

As for SO_4^{2-}/TiO_2 catalysts, increasing calcination temperature led to slightly decreased Cr(VI) adsorption capacities and increased anatase contents at calcination temperature lower than 600 °C. This indicated that the enhanced catalytic activity of SO_4^{2-}/TiO_2-500 is resulted from increased crystallinity. Further increasing calcination temperature led to a marked decrease in the adsorption capacities of SO_4^{2-}/TiO_2 samples and increased anatase contents. Considering that marked desorption/decomposition of surface SO_4^{2-} was observed at calcination temperature higher than 550 °C (see Fig. 3), the lower catalytic activity of TiO_2-700 were tentatively ascribed to the markedly lower Cr(VI) adsorption amount and the desorption of surface SO_4^{2-}.

In comparison with TiO_2-400, the catalytic activities of sulfated TiO_2 catalysts with calcination temperature lower than 600 °C were slightly low although these SO_4^{2-}/TiO_2 catalysts showed higher Cr(VI) adsorption capacities. Note that the

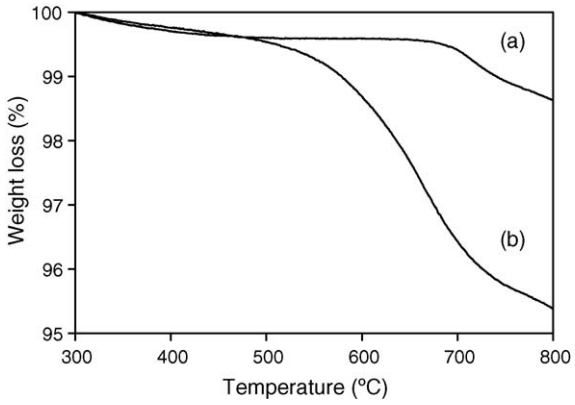

Fig. 8. Thermogravimetric (TG) curves of (a) SO_4^{2-}/TiO_2-500-W and (b) SO_4^{2-}/TiO_2-500.

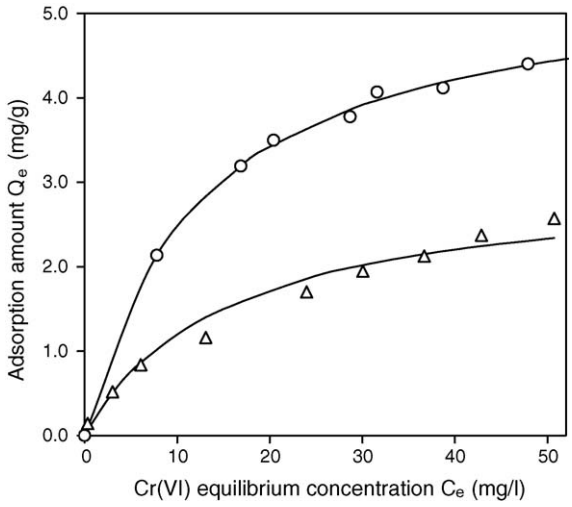

Fig. 9. Adsorption isotherms of Cr(VI) on (△) SO_4^{2-}/TiO_2-500 and (◯) SO_4^{2-}/TiO_2-500-W. Solid lines are theoretical fitting curves using Langmuir adsorption model.

crystalline degrees of these SO_4^{2-}/TiO_2 catalysts were lower compared to that of TiO_2-400, which suggests that the sulfation of TiO_2 hinders the crystallization of TiO_2 during the calcination process and simultaneously reduces their catalytic activities to some degree.

3.4. Role of surface SO_4^{2-}

It was generally accepted that the sulfation of TiO_2 hindered the growth of TiO_2 crystallites and the transformation of the crystalline phases [12,15]. A large amount of characterization results also demonstrated that both Brønsted and Lewis acid sites presented on the surface of sulfated TiO_2, indicating that the presence of SO_4^{2-} on the surface of TiO_2 increased the surface acidity of TiO_2 [45]. However, the straightforward evidences about the influence of the surface acidity on the catalytic activity of sulfated TiO_2 were scarce.

In principle, it is difficult to obtain the straightforward information about the roles of surface SO_4^{2-} by direct comparison of the TO_2 catalysts with their sulfated counterparts as the sulfation of TiO_2 also led to the changes in the structural properties of TiO_2. In order to clearly elucidate the influence of surface acidity on the photocatalytic activities of the SO_4^{2-}/TiO_2 samples for Cr(VI) reduction, SO_4^{2-}/TiO_2-500 was washed with Na_2CO_3 solution to remove the surface SO_4^{2-} species. Canton et al. [46] studied sulfated zirconia and quantitatively determined the content of SO_4^{2-} in sulfated zirconia samples by washing sulfated zirconia samples with an alkaline solution, which indicates that the SO_4^{2-} species on the metal oxides can be removed by the treatment using alkaline solution. XRD and UV-DRS results showed that the washing treatment did not lead to a change in the crystalline phase and textural properties compared with SO_4^{2-}/TiO_2-500. However, marked changes in the adsorption behavior, surface acidity and photocatalytic activity were observed.

After surface treatment, the residual amount of surface SO_4^{2-} was determined using TG analysis and the results were described in Fig. 8. For SO_4^{2-}/TiO_2-500, the surface SO_4^{2-} loss commenced at 500 °C. However, the surface SO_4^{2-} decomposition for SO_4^{2-}/TiO_2-500-W was observed at the calcination temperature higher than 680 °C. In addition, the amount of SO_4^{2-} loss in SO_4^{2-}/TiO_2-500-W was found to be approximately 1%, which is markedly lower compared to SO_4^{2-}/TiO_2-500 (about 4.2%). This pointed out that the surface treatment effectively removed SO_4^{2-} of SO_4^{2-}/TiO_2-500.

The adsorption isotherms of Cr(VI) on SO_4^{2-}/TiO_2-500-W and SO_4^{2-}/TiO_2-500 are compared in Fig. 9. Simulation using the Langmuir adsorption model showed that the maximum adsorption amount of Cr(VI) on SO_4^{2-}/TiO_2-500-W was 5.51 mg/g, which was markedly higher than that of SO_4^{2-}/TiO_2-500 (3.93 mg/g, see Table 2). This indicated that the surface treatment of SO_4^{2-}/TiO_2-500 using alkaline solution markedly increased the adsorption capacity of the sulfated TiO_2. Typically, SO_4^{2-} in the sulfated TiO_2 samples was anchored on the surface of TiO_2 to generate a complex with a bidentate sulfate ion structure via the surface hydroxyl groups of TiO_2 [10]. The treatment of SO_4^{2-}/TiO_2-500 with alkaline solution led to the release of the surface hydroxyl groups of TiO_2, which eventually elevated the adsorption capacity of SO_4^{2-}/TiO_2-500-W.

IR spectroscopy of pyridine adsorption and NH_3-TPD were used to characterize the change of the surface acidity before and after the washing treatment and the results are depicted in Figs. 10 and 11, respectively. For pyridine adsorption, IR bands at 1639, 1489, 1542, 1606, 1489 and 1445 cm^{-1} were observed in IR region 1700–1400 cm^{-1} after pyridine adsorption onto SO_4^{2-}/TiO_2-500 at room temperature. Among these IR bands, IR bands at 1542 and 1445 cm^{-1} are characteristic of pyridinium ions (pyridine interacting with Brønsted acid sites) and coordinatively bound pyridine (pyridine interacting with Lewis acid sites), respectively [47,48]. The intensities of these IR bands decreased upon degassing at 150 °C for 1 h. In particular, IR band at 1542 cm^{-1} still remained, indicating the presence of Brønsted acid sites in SO_4^{2-}/TiO_2-500. However, only IR bands at 1489, 1606, 1489 and 1445 cm^{-1} were observed after pyridine adsorption on SO_4^{2-}/TiO_2-500-W, indicating the absence of Brønsted acid sites in SO_4^{2-}/TiO_2-500-W. Note that the

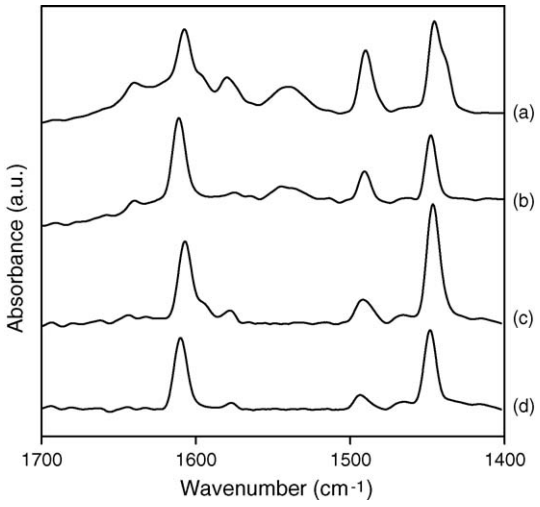

Fig. 10. IR spectra of pyridine adsorption on (a) SO_4^{2-}/TiO_2-500 at room temperature, (b) SO_4^{2-}/TiO_2-500 after degassing (a) at 150 °C for 1 h, (c) SO_4^{2-}/TiO_2-500-W at room temperature and (d) SO_4^{2-}/TiO_2-500-W after degassing (c) at 150 °C for 1 h. All spectra were recorded at room temperature.

surface Brønsted acid sites were resulted from the sulfation of TiO_2. Therefore, the results also clearly pointed out that the treatment of SO_4^{2-}/TiO_2-500 using Na_2CO_3 solution removes the surface Brønsted acid sites as well as the surface SO_4^{2-}.

NH_3-TPD results also supported above conclusions. For SO_4^{2-}/TiO_2-500 and SO_4^{2-}/TiO_2-500-W, NH_3 desorption peaks were detected between 200 and 450 °C, which indicates that weak and medium strong acid sites appear on the surface of these catalysts [16]. Integration results revealed that the area of NH_3 desorption peak from SO_4^{2-}/TiO_2-500 was approximately 2 times as large as that from SO_4^{2-}/TiO_2-500-W, which clearly indicates that the treatment of SO_4^{2-}/TiO_2-500 using Na_2CO_3 solution decreases the surface acidity of the sulfated TiO_2.

The photocatalytic activities of SO_4^{2-}/TiO_2-500-W and SO_4^{2-}/TiO_2-500 are compared in Fig. 12. It was found that UV irradiation for 180 min led to approximately 60% and 80% of Cr(VI) removal in the presence of SO_4^{2-}/TiO_2-500-W and SO_4^{2-}/TiO_2-500, respectively, which reveals that the partial

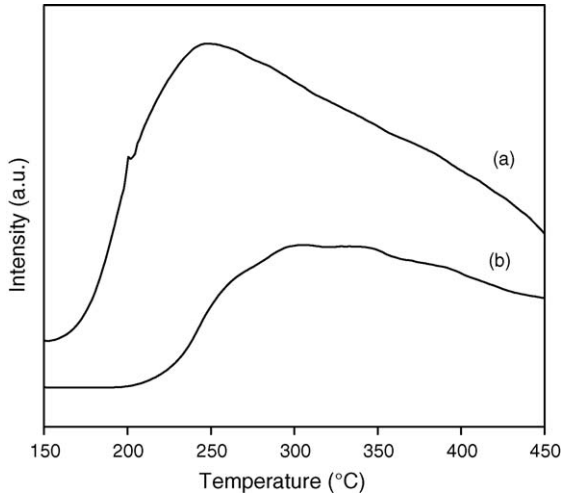

Fig. 11. NH_3-TPD profiles of (a) SO_4^{2-}/TiO_2-500 and (b) SO_4^{2-}/TiO_2-500-W.

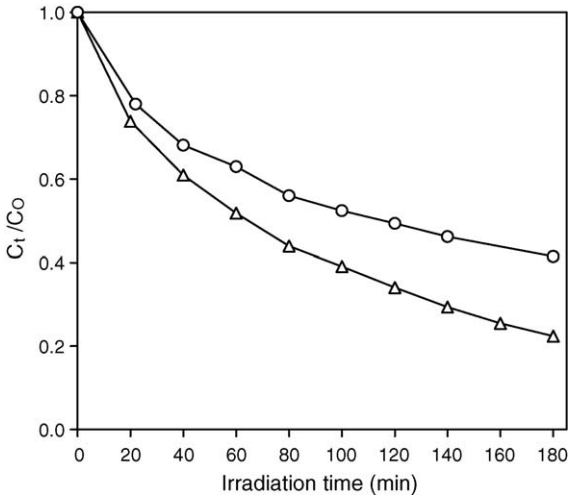

Fig. 12. Cr(VI) photo-reduction catalyzed by (△) SO_4^{2-}/TiO_2-500 and (◯) SO_4^{2-}/TiO_2-500-W. The pH value of solution was 2.5, initial concentration of Cr(VI) ion was 40 mg/l, dosage of catalyst was 1 g/l.

removal of surface sulfate species markedly diminishes the catalytic efficiency of SO_4^{2-}/TiO_2-500.

As for the influence of surface acidity on the catalytic activity of sulfated TiO_2, Gómez et al. [10] attributed the increased catalytic activity of sulfated TiO_2 for the photo-decomposition of 2,4-dinitroaniline to the effective trap of the excited electrons by the surface sulfate ions. For Cr(VI) photo-reduction, the apparent rate constants of SO_4^{2-}/TiO_2-500 and SO_4^{2-}/TiO_2-500-W were found to be 0.0079 and 0.0046 min^{-1}, respectively, which indicates that the removal of the surface acidity markedly diminishes the catalytic efficiency. The higher catalytic activity of SO_4^{2-}/TiO_2-500 compared to SO_4^{2-}/TiO_2-500-W also suggests that the trap of the excited electrons by the surface sulfate ions probably does not occur in our reaction system as the high catalytic efficiency for Cr(VI) photo-reduction is due to the effective utilization of the excited electrons. Note that the Cr(VI) reduction shifts to anode value with the decrease of pH value [49]. In parallel, Ku and Jung [33] also observed that the efficiency of Cr(VI) photo-reduction was markedly higher at lower pH. Zheng et al. [20] studied the photo-reduction of Cr(VI) catalyzed by $K_2Ti_4O_9$ and contributed the enhanced catalytic efficiency of H^+-$K_2Ti_4O_9$ to its increased surface acidity compared with $K_2Ti_4O_9$. Therefore, it could be concluded that the surface acid sites of the sulfated TiO_2 samples are involved in the Cr(VI) photo-reduction process and the acid environment of the catalyst surface may markedly facilitate the Cr(VI) photo-reduction.

4. Conclusions

The catalytic activities of the TiO_2 and SO_4^{2-}/TiO_2 catalysts for Cr(VI) photo-reduction are dependent on their adsorption and textural properties. Increasing the calcination temperature leads to the growth of crystallites, decrease of the adsorption capacities and change of the crystalline contents of the catalysts. For the TiO_2 catalysts, the increase of anatase content enhances the catalytic efficiency for Cr(VI) photo-reduction. In

comparison with TiO_2 catalysts, the presence of SO_4^{2-} on the surface of TiO_2 substantially preserves the adsorption capacities of the sulfated TiO_2 catalysts during the calcination process. However, sulfation of TiO_2 leads to a lower crystallinity degree, which eventually results in a slightly lower catalytic activity of SO_4^{2-}/TiO_2 catalysts compared to TiO_2 catalysts under calcination temperature lower than 400 °C. The higher catalytic activities of sulfated TiO_2 catalysts than TiO_2 catalysts can be only achieved at calcination temperature above 500 °C. In addition, the presence of the surface acid sites on the sulfated TiO_2 catalysts provides an acid environment over the catalyst surface and thus favors the photo-reduction of Cr(VI). Based on our research results, effectively increasing the content of anatase in the sulfated TiO_2 catalysts using other synthesis method can be expected to further enhance their catalytic activities for Cr(VI) photo-reduction.

Acknowledgement

The Advanced Analytical Center of Nanjing University is gratefully acknowledged for financial support.

References

[1] M.R. Hoffmann, S.T. Martin, W. Choi, D.W. Bahnemann, Environmental applications of semiconductor photocatalysis, Chem. Rev. 95 (1995) 69–96.
[2] A. Fujishima, T.N. Rao, D.A. Tryk, Titanium dioxide photocatalysis, J. Photochem. Photobiol. C 1 (2000) 1–21.
[3] M. Karkmaz, E. Puzenat, C. Guillard, J.M. Herrmann, Photocatalytic degradation of the alimentary azo dye amaranth Mineralization of the azo grroup to nitrogen, Appl. Catal. B 51 (2004) 183–194.
[4] S. Sato, T. Kadowaki, Photocatalytic activities of metal oxide semiconductors for oxygen isotope exchange and oxidation reactions, J. Catal. 106 (1987) 295–300.
[5] S. Malato, J. Blanco, C. Richter, M.I. Maldonado, Optimization of preindustrial solar photocatalytic mineralization of commercial pesticides: application to pesticide container recycling, Appl. Catal. B 25 (2000) 31–38.
[6] I.K. Konstantinou, T.M. Sakellarides, V.A. Sakkas, T.A. Albanis, Photocatalytic degradation of selected s-triazine herbicides and organophosphorus insecticides over aqueous TiO_2 suspensions, Environ. Sci. Technol. 35 (2001) 398–405.
[7] P. Mohapatra, S.K. Samantaray, K. Parida, Photocatalytic reduction of hexavalent chromium in aqueous solution over sulphate modified titania, J. Photochem. Photobiol. A 170 (2005) 189–194.
[8] G. Colón, M.C. Hidalgo, M. Macias, J.A. Navio, Enhancement of TiO_2/C photocatalytic activity by sulfate promotion, Appl. Catal. A 259 (2004) 235–243.
[9] D. Dvoranová, V. Brezová, M. Mazur, M.A. Malati, Investigations of metal-doped titanium dioxide photocatalysts, Appl. Catal. B 37 (2002) 91–105.
[10] R. Gómez, T. López, E. Ortiz-Islas, J. Navarrete, E. Sanchez, F. Tzompanztzi, X. Bokhimi, Effect of sulfation on the photoactivity of TiO_2 sol–gel derived catalysts, J. Mol. Catal. A 193 (2003) 217–226.
[11] S.K. Samantaray, P. Mohapatra, K. Parida, Physico-chemical characterisation and photocatalytic activity of nanosized SO_4^{2-}/TiO_2 towards degradation of 4-nitrophenol, J. Mol. Catal. A 198 (2003) 277–287.
[12] G. Colón, M.C. Hidalgo, J.A. Navio, Photocatalytic behaviour of sulphated TiO_2 for phenol degradation, Appl. Catal. B 45 (2003) 39–50.
[13] A.L. Linsebigler, G. Lu, J.T. Yates Jr., Photocatalysis on TiO_2 surfaces: principles, mechanisms, and selected results, Chem. Rev. 95 (1995) 735–758.
[14] C. Xie, Z. Xu, Q. Yang, N. Li, D. Zhao, D. Wang, Y. Du, Comparative studies of heterogeneous photocatalytic oxidation of heptane and toluene on pure titania, titania–silica mixed oxides and sulfated titania, J. Mol. Catal. A 217 (2004) 193–201.
[15] S. Yamazaki, N. Fujinaga, K. Araki, Effect of sulfate ions for sol–gel synthesis of titania photocatalyst, Appl. Catal. A 210 (2001) 97–102.
[16] Z. Ma, Y. Yue, X. Deng, Z. Gao, Nanosized anatase TiO_2 as precursor for preparation of sulfated titania catalysts, J. Mol. Catal. A 178 (2002) 97–104.
[17] J. Kotas, Z. Stasicka, Chromium occurrence in the environment and methods of its speciation, Environ. Pollut. 107 (2000) 263–283.
[18] B. Sun, E.P. Reddy, P.G. Smirniotis, Visible light Cr(VI) reduction and organic chemical oxidation by TiO_2 photocatalysis, Environ. Sci. Technol. 39 (2005) 6251–6259.
[19] C.R. Chenthamarakshan, K. Rajeshwar, E.J. Wolfrum, Heterogeneous photocatalytic reduction of Cr(VI) in UV-irradiated titania suspensions: effect of protons, ammonium ions, and other interfacial aspects, Langmuir 16 (2000) 2715–2721.
[20] S. Zheng, D. Yin, W. Miao, G.K. Anderson, Cr(VI) photoreduction catalysed by ion-exchangeable layered compounds, J. Photochem. Photobiol. A 117 (1998) 105–109.
[21] S.G. Schrank, H.J. José, R.F.P.M. Moreira, Simultaneous photocatalytic Cr(VI) reduction and dye oxidation in a TiO_2 slurry reactor, J. Photochem. Photobiol. A 147 (2002) 71–76.
[22] J.J. Testa, M.A. Grela, M.I. Litter, Heterogeneous photocatalytic reduction of chromium(VI) over TiO_2 particles in the presence of oxalate: involvement of Cr(V) species, Environ. Sci. Technol. 38 (2004) 1589–1594.
[23] B. Ohtani, Y. Ogawa, S. Nishimoto, Photocatalytic activity of amorphous–anatase mixture of titanium(IV) oxide particles suspended in aqueous solutions, J. Phys. Chem. B 101 (1997) 3746–3752.
[24] H. Zhang, J.F. Banfield, Understanding polymorphic phase transformation behavior during growth of nanocrystalline aggregates: insights from TiO_2, J. Phys. Chem. B 104 (2000) 3481–3487.
[25] J. Lin, Y. Lin, P. Liu, M.J. Meziani, L.F. Allard, Y.J. Sun, Hot-fluid annealing for crystalline titanium dioxide nanoparticles in stable suspension, J. Am. Chem. Soc. 124 (2002) 11514–11518.
[26] R. Srinivasan, R.A. Keogh, D.R. Milburn, B.H. Davis, Sulfated zirconia catalysts characterization by TGA/DTA/Mass spectrometry, J. Catal. 153 (1995) 123–130.
[27] M.A. Fox, M.T. Dulay, Heterogeneous photocatalysis, Chem. Rev. 93 (1993) 341–357.
[28] P. Zamostny, Z. Belohlav, Identification of kinetic models of heterogeneously catalyzed reactions, Appl. Catal. A 225 (2002) 291–299.
[29] N.J. Peill, M.R. Hoffmann, Mathematical model of a photocatalytic fiber-optic cable reactor for heterogeneous photocatalysis, Environ. Sci. Technol. 32 (1998) 398–404.
[30] A. Houas, H. Lachheb, M. Ksibi, E. Elaloui, C. Guillard, J.-M. Hermann, Photocatalytic degradation pathway of methylene blue in water, Appl. Catal. B 31 (2001) 145–157.
[31] H.Y. Chen, O. Zahraa, M. Bouchy, F. Thomas, J.Y. Bottero, Adsorption properties of TiO_2 related to the photocatalytic degradation of organic contaminants in water, J. Photochem. Photobiol. A 85 (1995) 179–186.
[32] Y. Oosawa, M. Gratzel, Effect of surface hydroxyl density on photocatalytic oxygen generation in aqueous TiO_2 suspensions., J. Chem. Soc., Faraday Trans. 84 (1988) 197–205.
[33] Y. Ku, I. Jung, Photocatalytic reduction of Cr(VI) in aqueous solutions by UV irradiation with the presence of titanium dioxide, Water Res. 35 (2001) 135–142.
[34] C.H. Weng, J.H. Wang, C.P. Huang, Adsorption of Cr(VI) onto TiO_2 from dilute aqueous solutions, Water Sci. Technol. 35 (1997) 55–62.
[35] H.P. Boehm, M. Herrmann, Über die Chemie der Oberfläche des Titandioxids. I. Bestimmung des aktiven Wasserstoffs, thermische Entwässerung und Rehydroxylierung, Z. Anorg. Allgem. Chem. 352 (1967) 156–167.
[36] T. López, E. Sánchez, P. Bosch, Y. Meas, R. Gómez, FT-IR and UV–vis(diffuse reflectance) spectroscopic characterization of TiO_2 sol–gel, Mater. Chem. Phys. 32 (1992) 141–152.

[37] L.A.G. Rodenas, A.D. Weisz, G.E. Magaz, M.A. Blesa, Effect of light on the electrokinetic behavior of TiO_2 particles in contact with Cr(VI) aqueous solutions, J. Colloid Interface Sci. 230 (2000) 181–185.

[38] J.J. Testa, M.A. Grela, M.I. Litter, Experimental evidence in favor of an initial one-electron-transfer process in the heterogeneous photocatalytic reduction of chromium(VI) over TiO_2, Langmuir 17 (2001) 3515–3517.

[39] Y. Kera, H. Kominami, S. Murakami, B. Ohtani, Design, preparation and characterization of highly active metal oxide photocatalysts, in: K. Masao, O. Ichiro (Eds.), Photocatalysis: Science and Technology, Springer, 2003, pp. 29–33.

[40] B. Ohtani, Y. Okugawa, S. Nishimoto, T. Kagiya, Photocatalytic activity of TiO_2 powders suspended in aqueous silver nitrate solution correlation with pH-dependent surface structures, J. Phys. Chem. 91 (1987) 3550–3555.

[41] T. Sreethawong, Y. Suzuki, S. Yoshikawa, Synthesis, characterization, and photocatalytic activity for hydrogen evolution of nanocrystalline mesoporous titania prepared by surfactant-assisted templating sol–gel process, J. Solid State Chem. 178 (2005) 329–338.

[42] T. Ohno, K. Tokieda, S. Higashida, M. Matsumura, Synergism between rutile and anatase TiO_2 particles in photocatalytic oxidation of naphthalene, Appl. Catal. A 244 (2003) 383–391.

[43] T. Ohno, K. Sarukawa, K. Tokieda, M. Matsumura, Morphology of a TiO_2 photocatalyst (Degussa, P-25) consisting of anatase and rutile crystalline phase, J. Catal. 203 (2001) 82–86.

[44] M. Yan, F. Chen, J. Zhang, M. Anpo, Preparation of controllable crystalline titania and study on the photocatalytic properties, J. Phys. Chem. B 109 (2005) 8673–8678.

[45] L.K. Noda, R.M. de Almeida, N.S. Goncalves, L.F.D. Probst, O. Sala, TiO_2 with a high sulfate content-thermogravimetric analysis, determination of acid sites by infrared spectroscopy and catalytic activity, Catal. Today 85 (2003) 69–74.

[46] P. Canton, R. Olindo, F. Pinna, G. Strukul, P. Riello, M. Meneghetti, G. Cerrato, C. Morterra, A. Benedetti, Alumina-promoted sulfated zirconia system: structure and microstructure characterization, Chem. Mater. 13 (2001) 1634–1641.

[47] C.A. Emeis, Determination of integrated molar extinction coefficients for infrared absorption bands of pyridine adsorbed on solid acid catalysts, J. Catal. 141 (1993) 347–354.

[48] V.P. Glazunov, S.E. Odinokov, Infrared spectra of pyridinium salts in solution. I. The region of middle frequencies, Spectrochim. Acta 38A (1982) 399–408.

[49] G.D. Christian, Analytical Chemistry, John Wiley & Sons, New York, 1980.